Interspeech 2024
1-5 September 2024, Kos, Greece

Modeling Vocal Tract Like Acoustic Tubes Using the Immersed Boundary Method

Rongshuai Wu[1], *Debasish Ray Mohapatra*[1], *Sidney Fels*[1]

[1]Department of Electrical and Computer Engineering, University of British Columbia, Canada

rowansh@student.ubc.ca, debasishray@ece.ubc.ca, ssfels@ece.ubc.ca

Abstract

The standard finite-difference time-domain (FDTD) wave solver employs a regular grid that approximates vocal tract boundaries in a stair-stepped manner, making it less effective for modeling complex and dynamic geometry. We present a novel 2D wave solver that integrates a unique immersed boundary method with FDTD, enabling precise approximation of wave propagation in acoustic tubes. The solver uses Lagrangian points to define vocal tract boundaries on a regular grid, eliminating their stair-stepped discretization. The boundary and the flow equations interact via additional forcing terms characterized by boundary immittances. The results show that the formant frequencies of a single-segment tube closely align with its analytical solutions, exhibiting a percentage deviation of less than 3%. Similarly, the frequency responses of a two-segment tube and actual vocal tract geometries show good agreement with existing state-of-the-art 2D and 3D wave solvers, except for a few discrepancies.

Index Terms: articulatory speech synthesis, vocal tract, immersed boundary method, FDTD, computational acoustic

1. Introduction

Computational modeling of the upper airway presents several challenges due to the complex geometry of the vocal tract cavity that connects the larynx to the mouth opening. Additionally, modeling the fluid-structure interaction between the airflow and moving vocal tract boundary demands advanced computational techniques. The conventional approach to the vocal tract modeling involves employing a regular Cartesian grid that conforms to its boundary in a stair-stepped manner [1, 2, 3], which is ideal for accelerating the acoustic wave solver [4]. It also enables the straightforward implementation of essential boundary conditions by directly changing the grid cell properties [3]. Nevertheless, this method necessitates high spatiotemporal resolution to reduce the discretization error of complex geometries [2, 5], and also affects numerical stability while modeling dynamic vocal tracts due to frequent transformation of grid cell properties close to the surface boundary [6, 7].

An alternative approach to sidestepping the need for meshing boundary surfaces by employing grid cells is through the use of immersed boundary methods (IBMs) [8, 9]. The distinctive feature of IBM lies in carrying out simulations on a Cartesian grid that does not need to conform to the boundaries of the simulated bodies, thereby entirely avoiding the stair-stepped discretization error in complex geometries [10]. IBM employs a set of Lagrangian markers or points distributed throughout the computational domain to describe the immersed surface of a body. The immersed body (IB) then interacts with the underlying fluid flow, defined using a Cartesian grid, by adding forcing terms to the wave equations.

Peskin first developed the IB technique [11] to simulate cardiac mechanics and associated blood flow. Since then, several variants of this approach have been proposed to solve various fluid-structure interaction problems, typically involving nonlinear flow and complex boundaries [9, 12, 13, 14]. In the realm of speech synthesis applications, IBMs have primarily been used for modeling vocal fold vibration in the larynx [15, 16]. Recently, Wei et al. [7] utilized IBM to propose a novel wave solver for modeling vocal tract acoustics. The solver introduces a force field exclusively to the momentum equation, which is calculated at the Lagrangian points situated along the vocal tract boundary and then extrapolated to the nearby Eulerian grid cells to account for fluid-structure interactions. The wave equations are subsequently solved using a 2D Finite-Difference Time-Domain (FDTD) numerical scheme. However, the added force field is independent of wall impedance, which makes modeling the vocal tract wall losses challenging. These losses significantly influence the formant frequencies and bandwidth of vocal tract transfer functions [17]. Additionally, the spectral features of Wei's acoustic wave solver were not validated against state-of-the-art vocal tract models.

To overcome these limitations, we introduce a novel vocal tract model that employs a unique IBM, previously used for virtual and room acoustics modeling [10, 18], to seamlessly immerse vocal tract contours within a 2D Cartesian grid. The model then takes advantage of the 2D FDTD scheme to discretize the governing wave equations and approximate the acoustic wave propagation. Unlike Wei's wave solver, our proposed model incorporates a couple of discrete forcing terms obtained from the Lagrangian points of the immersed vocal tract contours into the both Eulerian momentum and mass equations. The inclusion of these forcing terms, characterized by distinct immittances, allows the precise modeling of vocal tract boundary conditions, thus enhancing the spectral features of synthesized acoustic output. As we use a regular computational grid for the acoustic fluid simulation, the parallelization and numerical stability condition of the FDTD wave solver remains undisturbed [10]. The accuracy of our proposed model is validated using three types of acoustic tubes resembling vocal tracts, each exhibiting varying degrees of geometrical complexity. To assess the model, transfer functions are compared against those derived from an extended 2D FDTD model [1] and a highly accurate 3D Finite Element (FE) model [19].

2. Method

2.1. Acoustics Wave Equations

Consider an air medium having uniform density ρ confined to a two-dimensional (2D) space, specifically the x/y plane. Sup-

10.21437/Interspeech.2024-2087

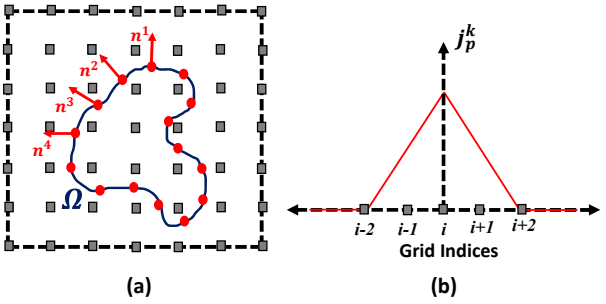


Figure 1: *(a) A 2D contour Ω immersed in $\mathbb{R}^2$, defined using K Lagrangian points (red dots) and normal vectors n^k. (b) Triangular kernel function j_p^k to approximate the Dirac Delta function over grid cells.*

pose at time t, an infinitesimally small fluid particle located in the medium at $\boldsymbol{X}$ moves in response to an external force. As discussed later, this force could be prescribed using a source excitation function with a velocity of u_s. Consequently, the spatiotemporal evolution of pressure p and particle velocity $\boldsymbol{v}$ within the medium can be approximated by a system of Eulerized linear wave equations [7] as follows,

$$\frac{1}{\rho c^2}\frac{\partial p}{\partial t} + \boldsymbol{\nabla}\cdot\boldsymbol{v} = \delta^{(2)}(\boldsymbol{X}-\boldsymbol{X_s})u_s \quad (1)$$

$$\rho\frac{\partial \boldsymbol{v}}{\partial t} + \boldsymbol{\nabla}p = 0 \quad (2)$$

with: $\boldsymbol{v} = (v_x, v_y)$ and $\boldsymbol{X} \in \mathbb{R}^2$

Here, v_x and v_y are the vector components of the particle velocity, and c is the sound speed. The 2D Dirac delta function $\delta^{(2)}(\boldsymbol{X}-\boldsymbol{X_s})$ introduces an external source velocity at a position $\boldsymbol{X} = \boldsymbol{X_s}$ within the computation domain. $\boldsymbol{\nabla}$ and $\boldsymbol{\nabla}\cdot$ represent the 2D gradient and divergence operations, respectively. These wave equations can be used to model sound resonances and radiation in acoustic tubes, such as vocal tracts [1] and musical instruments [20].

2.2. Immersed Boundary Method

2.2.1. Immersed Boundary

Let us consider the sagittal contour (i.e., the immersed boundary) $\Omega \subset \mathbb{R}^2$ of a body, defined on a 2D Cartesian grid, consists of K distinct Lagrangian points, as shown in Figure 1a. These points are positioned at coordinates $\boldsymbol{\xi}$ within the Lagrangian space Ω. Associated with each point is a normal vector $n(\boldsymbol{\xi})$, oriented perpendicularly to the body contour. Then the Equations 1 and 2 can be updated for the immersed boundary condition using a pair of forcing terms as described in [21],

$$\frac{1}{\rho c^2}\frac{\partial p}{\partial t} + \boldsymbol{\nabla}\cdot\boldsymbol{v} + \int_\Omega v_\Delta(\boldsymbol{\xi},t)\delta^{(2)}(\boldsymbol{X}-\boldsymbol{\xi})d\boldsymbol{\xi} = \delta^{(2)}(\boldsymbol{X}-\boldsymbol{X_s})u_s \quad (3)$$

$$\rho\frac{\partial \boldsymbol{v}}{\partial t} + \boldsymbol{\nabla}p + \int_\Omega p_\Delta(\boldsymbol{\xi},t)\boldsymbol{n}(\boldsymbol{\xi})\delta^{(2)}(\boldsymbol{X}-\boldsymbol{\xi})d\boldsymbol{\xi} = 0 \quad (4)$$

Here, the scalar forcing functions $v_\Delta(\boldsymbol{\xi},t)$ and $p_\Delta(\boldsymbol{\xi},t)$, defined at each Lagrangian point coordinate $\boldsymbol{\xi}$, helps in representing passive vocal tract boundaries and coupling the airflow with that of the immersed boundary. In acoustic applications, such forcing functions can also be expressed in terms of immittances in the Laplace domain as follows [22],

$$\hat{p}_\Delta(\boldsymbol{\xi},s) = 2Z_0 Z_d \hat{\hat{v}}(\boldsymbol{\xi},s) \quad (5)$$

$$\hat{v}_\Delta(\boldsymbol{\xi},s) = 2Y_0 Y_m \hat{\hat{p}}(\boldsymbol{\xi},s) \quad (6)$$

Here, $\bar{p}$ and $\bar{v}$ are the average pressures and velocities at the immersed surface, respectively. Using these interpolated average field variables, the forcing functions can be derived from the acoustic parameters of the wave equations, defined in the Cartesian grid (see the next subsection). Z_0 and Y_0 represent the characteristic impedance and admittance of air, respectively. $Z_d = 1/Y_m$ is defined as the impedance of the immersed surface. The value of Z_d is set as proposed by Yokota et al. [23], and the vocal tract contours are simulated by adapting the local reactive boundary approach. This approach is in line with the work of Takemoto et al. [3] for modeling vocal tract wall absorption. Prior to interpolation and discretization, Equations 3 and 4 can be approximated by a sum of a finite number of point forcing functions as follows,

$$\frac{1}{\rho c^2}\frac{\partial p}{\partial t} + \boldsymbol{\nabla}\cdot\boldsymbol{v} + \sum_{k=1}^{K} v_\Delta^k \delta^{(2)}(\boldsymbol{X}-\boldsymbol{\xi}^k)S^k = \delta^{(2)}(\boldsymbol{X}-\boldsymbol{X_s})u_s \quad (7)$$

$$\rho\frac{\partial \boldsymbol{v}}{\partial t} + \boldsymbol{\nabla}p + \sum_{k=1}^{K} p_\Delta^k \boldsymbol{n}^k \delta^{(2)}(\boldsymbol{X}-\boldsymbol{\xi}^k)S^k = 0 \quad (8)$$

where, k represents k^{th} Lagrangian point on contour Ω, and S^k represents the boundary segment length at k^{th} point.

2.2.2. Forcing Functions Interpolation

In general, the coordinates of Lagrangian points $\boldsymbol{\xi}$ do not coincide with the Eulerian points $\boldsymbol{X}$. Therefore, to model the fluid-structure interactions [10], the forcing functions on an immersed surface need to be derived directly from the acoustic field parameters through their dependence on average field variables $\bar{p}$ and $\bar{v}$ (shown in Equations 5 and 6), defined as follows,

$$\bar{p}^k = \iint_{\mathbb{R}^2} p(\boldsymbol{X},t)\delta^{(2)}(\boldsymbol{X}-\boldsymbol{\xi}^k)d\boldsymbol{X} \quad (9)$$

$$\bar{v}^k(t) = \boldsymbol{n}^k \cdot \iint_{\mathbb{R}^2} v(\boldsymbol{X},t)\delta^{(2)}(\boldsymbol{X}-\boldsymbol{\xi}^k)d\boldsymbol{X} \quad (10)$$

These equations effectively perform an *interpolation* operation by using 2D Dirac delta functions and compute a weighted average of p and v over the adjacent Cartesian grid cells, which yields the corresponding $\bar{p}$ and $\bar{v}$ at each Lagrangian point.

2.2.3. Discrete Approximation to the Dirac Delta Function

A smoothed approximation to the 2D Dirac delta function is required since it has been used both in the forcing terms (Equations 7 and 8) and the interpolation operation (Equations 9 and 10). It also arises in the discrete representation of the source term as shown in Equation 1. Therefore, we have employed a non-negative Triangular distribution function (illustrated in Figure 1b) to smoothly discretize the Dirac delta function over

the computational grid, adopting a similar approach to that proposed by Bilbao [21].

To demonstrate this process, let us consider equation 9, which requires an approximation to the Dirac delta function at the k^{th} Lagrangian point over the pressure grid. This approximation can be represented as a grid function j_p^k that contains values from the Triangular distribution and is defined using an $N_p \times 1$ vector. Here, N_p represents the number of pressure grid points. The grid function j_p^k must satisfy the moment condition [24], ensuring that the sum of all elements in j_p^k equals unity. Given that there are K Lagrangian points, we can arrange these vectors into an $N_p \times K$ matrix, denoted as $\boldsymbol{J_p} = \left[j_p^1, \ldots, j_p^K\right]$. A similar approach can also be followed to approximate the Dirac delta function for the velocity components (v_x and v_y) and the source term u_s as discussed by Bilbao. They can be denoted as $\boldsymbol{J_{v_x}}$, $\boldsymbol{J_{v_y}}$ and $\boldsymbol{J_s}$, respectively. $\boldsymbol{J_{v_x}}$ and $\boldsymbol{J_{v_y}}$ incorporate the components of normal vector n^k as well. Updating the interpolation Equations 9 and 10 with the discrete approximation of Dirac Delta function yields,

$$\bar{p} = \boldsymbol{J_p}^T p \tag{11}$$

$$\bar{v} = \boldsymbol{J_v}^T v \tag{12}$$

with: $\boldsymbol{J_v} = (\boldsymbol{J_{v_x}}, \boldsymbol{J_{v_y}})$

The continuous form of updated wave equations with immersed boundary conditions can be derived by substituting Equations 5, 6, 11, and 12 into Equations 7 and 8 as follows:

$$\frac{1}{\rho c^2}\frac{\partial p}{\partial t} + \boldsymbol{\nabla} \cdot \boldsymbol{v} + 2Mp = \boldsymbol{J_s} u_s \tag{13}$$

$$\rho \frac{\partial \boldsymbol{v}}{\partial t} + \boldsymbol{\nabla} p + 2Nv = 0 \tag{14}$$

with: $M = Y_0 Y_m S^k J_p J_p^T$ and $N = Z_0 Z_d S^k J_v J_v^T$

2.3. FDTD Numerical Scheme

For the FDTD simulation, we employed the standard 2D Yee scheme, where the simulation grid is composed of square 2D cells [1, 25]. At each time step n, pressure values $p^{(n)}$ are recorded at the centers of these cells across the entire domain. Concurrently, the velocity vector components $v_x^{(n)}$ and $v_y^{(n)}$ are measured at the edges adjacent to the right and top neighboring cells, respectively. Therefore, within a specific cell located at discrete coordinates $(\hat{x},\ \hat{y})$, the pressure p is sampled at $(\hat{x},\ \hat{y})$, the velocity component v_x at $(\hat{x} + 1/2,\ \hat{y})$, and v_y at $(\hat{x},\ \hat{y} + 1/2)$. This leads to the following discrete update rules of Equations 13 and 14 in the vector-matrix form, where we denote $\widetilde{\nabla}$ with the standard discrete spatial derivatives as performed in FDTD and $\boldsymbol{I}$ with identity matrix.

$$p^{(n+1)} = (\boldsymbol{I} + M\rho c^2 \Delta t)^{-1}\Big[(\boldsymbol{I} - M\rho c^2 \Delta t)p^{(n)} + \rho c^2 \Delta t \boldsymbol{J_s} u_s^{(n)} - \rho c^2 \Delta t\, \widetilde{\boldsymbol{\nabla}} \cdot \boldsymbol{V}^{(n)}\Big] \tag{15}$$

$$\boldsymbol{v}^{(n+1)} = (\boldsymbol{I} + N\Delta t/\rho)^{-1}\Big[(\boldsymbol{I} - N\Delta t/\rho)v^{(n)} - \Delta t\, \widetilde{\nabla} p^{(n+1)}/\rho\Big] \tag{16}$$

Our solution procedure to obtain the $p^{(n+1)}$ and $v^{(n+1)}$ at each time step is as follows:

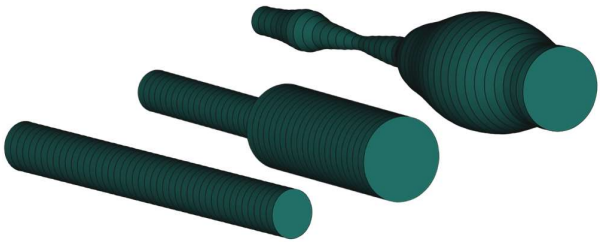


Figure 2: *Illustration of single-segment, two-segment and vocal tract geometries (left to right).*

1. Extract the 2D contour from a scaled 3D tube area functions, as described by Arnela and colleagues (2014). Define this contour in a 2D Eulerian grid using a set of Lagrangian points with coordinates ξ.
2. Before starting the simulation, initialize the acoustic parameters $p^{(n)}$ and $v^{(n)}$ to zero.
3. For each Lagrangian point, interpolate the forcing terms from the surrounding grid cells' acoustic parameters to compute M, N, and $\boldsymbol{J_s}$ matrices.
4. Update the source velocity u_s by using a source excitation function.
5. Update the pressure $p^{(n+1)}$ and velocity components $v^{(n+1)}$ by extrapolating the pressure and velocity at the Lagrangian points to the adjacent Eulerian grid cells.
6. Iterate steps 3 through 5 for the entire simulation duration.

3. Experiments & Results

3.1. Model Evaluation

We evaluated the acoustic characteristics of the proposed model (2D IBM) by using an extended 2D FDTD [1] model and a high-accuracy 3D Finite Element model (3D FEM [19]) as references. To this end, we compared their transfer functions for three types of acoustic tubes that resemble human vocal tracts. Figure 2 shows the geometrical complexity of these tubes.

First, we validated our model for a cylindrical tube by comparing its obtained resonance frequencies with the corresponding analytical solution. This tube, designed with a length of $L = 170$ mm and an internal diameter of $d = 14.5$ mm, aimed to roughly approximate the vocal tract length of vowel /a/ for a male speaker [19, 26]. Subsequently, we increased the tube's geometrical complexity by approximating the vocal tract using two waveguide sections [27]. Each section had a length of $L = 85$ mm, with internal diameters of $d_1 = 14.5$ mm and $d_2 = 29.5$ mm. Lastly, we evaluated our model for actual vocal tract geometries derived through MR imaging of the vowel sounds /a/, /i/ and /u/ [28]. These vocal tracts are composed of 44 juxtaposed cylindrical segments with varying cross-sectional areas. For simplicity, we will henceforth refer to these tubes as single-segment, two-segment, and vocal tract geometries. We directly compared the transfer functions of two-segment and vocal tract models to those derived from the 2D FDTD and 3D FEM simulations.

3.2. Experimental Setup

For all simulations, we set the sound speed to $c = 350$ m/s and air density to $\rho = 1.14$ kg/m^3. We empirically fine-tuned the boundary admittance of the proposed model to match the formant bandwidths of the 3D FEM solution. For the FEM simula-

tion, we set the mesh size to 2.5 mm. For optimal performance, the spatial resolution of the Cartesian grid (Δs) in the 2D FDTD and IBM models was set to 1.1 mm and 0.74 mm, respectively. For numerical stability, the corresponding temporal resolution was derived using the Courant-Friedrichs-Lewy (CFL) condition, i.e., $\Delta t \leq \Delta s/\sqrt{2}c$, as in standard 2D FDTD simulations. As proposed in [29], we maintained the distance between two adjacent Lagrangian points at less than $\Delta s/2$. We ran the 3D FE simulations with a mesh size of 2.5 mm and temporal resolution of $\Delta t = 5 \times 10^{-6}$ s. For the 2D FDTD model, the spatial resolution was set to 0.75 mm. While generating the sagittal vocal tract boundaries inside the Eulerian computational domain for the 2D IBM model, we constrained the distance between the upper and lower boundary to a minimum value of $2\Delta s$ to avoid boundary interference.

In all three models (3D FEM, 2D FDTD and 2D IBM), a Gaussian band-pass filter was applied at the start of the tube as a source excitation function [3]. Additionally, a Dirichlet boundary condition ($p = 0$) was enforced at the tube end for open-end termination. A virtual microphone was placed at 3 mm inside from the tube end to record pressure samples at each time step. Transfer functions were obtained up to 8 kHz using the recorded pressure samples to validate the proposed model. The duration for all simulations was set to 50 ms.

3.3. Results and Discussion

3.3.1. Single-segment Tube Model

The transfer function of the single-segment tube was obtained by applying the Fast Fourier Transform to the recorded pressure samples at the tube end. The first eight formants (i.e., resonance frequencies) were extracted from the transfer function and compared with the corresponding analytical solution. The analytical solution can be determined using the following equation [19], where n is the formant index and L is the tube length.

$$f = \frac{(2n-1)c}{4L} \tag{17}$$

Table 1 shows the formant frequency positions derived from the analytical calculations and the 2D IBM simulation. The formants obtained from the proposed model match well with the analytical solution with a maximum deviation of 1.0% and an average deviation of 0.5%. This level of accuracy suggests that the 2D IBM model can precisely simulate wave propagation and boundary immittances in simplified acoustic tubes.

Formants (f_n)	Analytical (in Hz)	2D IBM (in Hz)
f_1	514	520 (1.0%)
f_2	1544	1560 (1.0%)
f_3	2574	2580 (0.3%)
f_4	3603	3620 (0.5%)
f_5	4632	4660 (0.6%)
f_6	5662	5680 (0.3%)
f_7	6691	6700 (0.1%)
f_8	7721	7740 (0.3%)

Table 1: *The first eight formant frequencies of the single-segment tube model obtained by the analytical calculation and the proposed 2D IBM method. The percentage of formant position deviations is provided in blue color.*

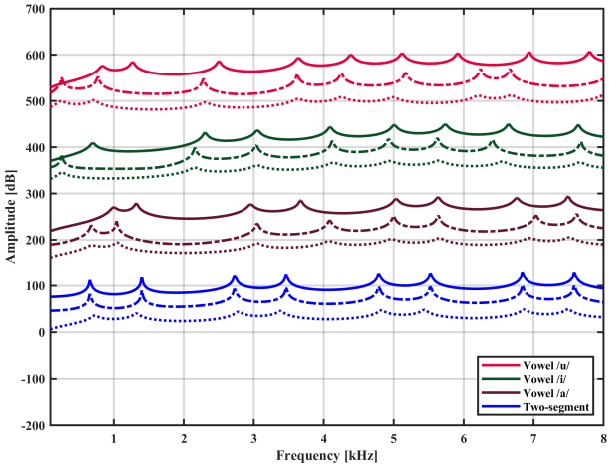


Figure 3: *Transfer functions of two-segment and vocal tract geometries (Vowels: /a/, /i/ and /u/) obtained with the 3D FEM (dotted lines), 2D FDTD (dashed lines) and 2D IBM (solid lines) simulations; Curves were offset manually.*

3.3.2. Two-segment Tube Model and Vocal Tract Models

As discussed in the preceding subsection, we examined the frequency responses of both two-segment tubes and the vocal tract geometries of three vowels using all three models. We compared their transfer functions to assess the efficacy of the proposed 2D Immersed Boundary Method (IBM) model, as illustrated in Figure 3. As anticipated, the transfer functions from the 2D IBM method exhibited a strong correlation with those obtained through 2D Finite-Difference Time-Domain (FDTD) and 3D Finite Element Method (FEM) simulations. For all vowels, the percentage deviation in formant frequencies above 3 kHz is less than 5% for the proposed 2D IBM model when compared to the highly precise 3D FEM and 2D FDTD models. However, for the vowels /i/ and /u/, some discrepancies were observed at lower frequencies, with deviations greater than 5%. These differences could be attributed to the narrow constrictions in their vocal tract geometry and can be reduced by increasing the sampling rate of the proposed wave solver [4].

4. Conclusion

In this study, we introduced a novel 2D Immersed Boundary Method (IBM) specifically designed to approximate the propagation of acoustic waves in tube geometries similar to the human vocal tract. This model, distinct from traditional Finite-Difference Time-Domain (FDTD) methods, employs Lagrangian points to model the tube boundary. The interaction between the boundary and airflow is captured using additional forcing terms. This approach facilitates the modeling of complex acoustic tubes, enabling the synthesis of a diverse array of speech sounds. Furthermore, our method offers the potential for extension to simulate dynamic changes in vocal tract geometries. Enhancing the model's efficiency through parallelization of the algorithm could lead to significant advancements in the field of articulatory speech synthesis.

5. Acknowledgement

This work is supported by the Natural Sciences and Engineering Research Council (NSERC) of Canada and the Canadian Institutes for Health Research (CIHR).

6. References

[1] D. R. Mohapatra, V. Zappi, and S. Fels, "An extended two-dimensional vocal tract model for fast acoustic simulation of single-axis symmetric three-dimensional tubes," *Proc. Interspeech 2019*, pp. 3760–3764, 2019.

[2] D. R. Mohapatra, M. Fleischer, V. Zappi, P. Birkholz, and S. Fels, "Three-dimensional finite-difference time-domain acoustic analysis of simplified vocal tract shapes," *Proc. Interspeech 2022*, pp. 764–768, 2022.

[3] H. Takemoto, P. Mokhtari, and T. Kitamura, "Acoustic analysis of the vocal tract during vowel production by finite-difference time-domain method," *The Journal of the Acoustical Society of America*, vol. 128, no. 6, pp. 3724–3738, 2010.

[4] V. Zappi, A. Vasuvedan, A. Allen, N. Raghuvanshi, and S. Fels, "Towards real-time two-dimensional wave propagation for articulatory speech synthesis," in *Proceedings of Meetings on Acoustics 171ASA*, vol. 26, no. 1. ASA, 2016, p. 045005.

[5] A. C. Cangellaris and D. B. Wright, "Analysis of the numerical error caused by the stair-stepped approximation of a conducting boundary in fdtd simulations of electromagnetic phenomena," *IEEE transactions on antennas and propagation*, vol. 39, no. 10, pp. 1518–1525, 1991.

[6] J. Wei, S. Wang, Q. Hou, J. Dang *et al.*, "Generalized finite difference time domain method and its application to acoustics," *Mathematical Problems in Engineering*, vol. 2015, 2015.

[7] J. Wei, W. Guan, D. Q. Hou, D. Pan, W. Lu, and J. Dang, "A new model for acoustic wave propagation and scattering in the vocal tract." in *INTERSPEECH*, 2016, pp. 3574–3578.

[8] R. Mittal and G. Iaccarino, "Immersed boundary methods," *Annu. Rev. Fluid Mech.*, vol. 37, pp. 239–261, 2005.

[9] W.-X. Huang and F.-B. Tian, "Recent trends and progress in the immersed boundary method," *Proceedings of the Institution of Mechanical Engineers, Part C: Journal of Mechanical Engineering Science*, vol. 233, no. 23-24, pp. 7617–7636, 2019.

[10] S. Bilbao, "Modeling impedance boundary conditions and acoustic barriers using the immersed boundary method: The one-dimensional case," *The Journal of the Acoustical Society of America*, vol. 153, no. 4, 2023.

[11] C. S. Peskin, "Flow patterns around heart valves: a numerical method," *Journal of computational physics*, vol. 10, no. 2, pp. 252–271, 1972.

[12] W.-X. Huang, S. J. Shin, and H. J. Sung, "Simulation of flexible filaments in a uniform flow by the immersed boundary method," *Journal of computational physics*, vol. 226, no. 2, pp. 2206–2228, 2007.

[13] W.-X. Huang, C. B. Chang, and H. J. Sung, "An improved penalty immersed boundary method for fluid–flexible body interaction," *Journal of Computational Physics*, vol. 230, no. 12, pp. 5061–5079, 2011.

[14] F. Sotiropoulos and X. Yang, "Immersed boundary methods for simulating fluid–structure interaction," *Progress in Aerospace Sciences*, vol. 65, pp. 1–21, 2014.

[15] X. Zheng, Q. Xue, R. Mittal, and S. Beilamowicz, "A coupled sharp-interface immersed boundary-finite-element method for flow-structure interaction with application to human phonation," *Journal of Biomechanical Engineering*, vol. 132, no. 11, p. 111003, 2010.

[16] H. Luo, R. Mittal, X. Zheng, S. A. Bielamowicz, R. J. Walsh, and J. K. Hahn, "An immersed-boundary method for flow–structure interaction in biological systems with application to phonation," *Journal of computational physics*, vol. 227, no. 22, pp. 9303–9332, 2008.

[17] M. Fleischer, S. Pinkert, W. Mattheus, A. Mainka, and D. Mürbe, "Formant frequencies and bandwidths of the vocal tract transfer function are affected by the mechanical impedance of the vocal tract wall," *Biomechanics and modeling in mechanobiology*, vol. 14, pp. 719–733, 2015.

[18] S. Bilbao, "Immersed boundary methods in wave-based virtual acoustics," *The Journal of the Acoustical Society of America*, vol. 151, no. 3, pp. 1627–1638, 2022.

[19] P. Birkholz, S. Kürbis, S. Stone, P. Häsner, R. Blandin, and M. Fleischer, "Printable 3d vocal tract shapes from mri data and their acoustic and aerodynamic properties," *Scientific data*, vol. 7, no. 1, p. 255, 2020.

[20] A. Allen and N. Raghuvanshi, "Aerophones in flatland: Interactive wave simulation of wind instruments," *ACM Transactions on Graphics (TOG)*, vol. 34, no. 4, pp. 1–11, 2015.

[21] S. Bilbao, "Impedance boundaries and transmission in wave-based acoustics using the immersed boundary method," in *International Congress on Acoustics*. International Commission for Acoustics (ICA), 2022.

[22] O. Brune, "Synthesis of a finite two-terminal network whose driving-point impedance is a prescribed function of frequency," Ph.D. dissertation, Massachusetts Institute of Technology, 1931.

[23] T. Yokota, S. Sakamoto, and H. Tachibana, "Visualization of sound propagation and scattering in rooms," *Acoustical science and technology*, vol. 23, no. 1, pp. 40–46, 2002.

[24] Y. Liu and Y. Mori, "Properties of discrete delta functions and local convergence of the immersed boundary method," *SIAM Journal on Numerical Analysis*, vol. 50, no. 6, pp. 2986–3015, 2012.

[25] K. Yee, "Numerical solution of initial boundary value problems involving maxwell's equations in isotropic media," *IEEE Transactions on antennas and propagation*, vol. 14, no. 3, pp. 302–307, 1966.

[26] R. Blandin, M. Arnela, R. Laboissière, X. Pelorson, O. Guasch, A. V. Hirtum, and X. Laval, "Effects of higher order propagation modes in vocal tract like geometries," *The Journal of the Acoustical Society of America*, vol. 137, no. 2, pp. 832–843, 2015.

[27] G. Fant, *Acoustic theory of speech production: with calculations based on X-ray studies of Russian articulations*. Walter de Gruyter, 1971, no. 2.

[28] B. H. Story, "Comparison of magnetic resonance imaging-based vocal tract area functions obtained from the same speaker in 1994 and 2002," *The Journal of the Acoustical Society of America*, vol. 123, no. 1, pp. 327–335, 2008.

[29] C. S. Peskin, "The immersed boundary method," *Acta numerica*, vol. 11, pp. 479–517, 2002.